Electronic Supplementary Information (ESI)

Ultrathin anion exchange membranes with improved OH^- transfer rate for high-performance AEMFCs

Wanjie Song[a,‡], Xian Liang[a,b,‡], Huaqing Zhang[a], Xiang Liu[a], Xin Zhang[a], Liang Wu[a], Xiaolin Ge[a,*], Tongwen Xu[a*]

[a] *CAS Key Laboratory of Soft Matter Chemistry, Collaborative Innovation Centre of Chemistry for Energy Materials, School of Chemistry and Material Science, University of Science and Technology of China, Hefei 230026, P.R. China*

[b] *School of Chemistry and Material Engineering Huainan Normal University Huainan, Anhui 232001, P. R. China*

* Corresponding Author: twxu@ustc.edu.cn, gexl@ustc.edu.cn

‡ Wanjie Song and Xian Liang contributed equally to this work

Contents

Nomenclature

AEMs	anion exchange membranes
AEMFCs	anion exchange membrane fuel cells
PPD	peak power density
TMHD	N,N,N',N'-Tetramethyl-1,6-hexanediamine
TFA	trifluoroacetic acid
TFSA	trifluoromethanesulfonic acid
DCM	dichloromethane
NMP	N-Methylpyrrolidone
DMF	N,N-Dimethylformamide
TMAQA	6-(dimethylamino)-N-ethyl-N,N-dimethylhexan-1-aminium bromide
NBS	N-bromosuccinimide
AIBN	azobisisobutyronitrile
BP	the product of the copolymerization of dimethylbiphenyl, diphenyl and trifluoroacetone
BrBP	bromine of BP copolymers
QABP	quaternary aminated BrBP with TMAQA
BQAPPO	quaternary aminated poly(2,6-dimethyl-1,4-phenylene oxide) with TMAQA
DI	deionized
^{1}H NMR	proton nuclear magnetic resonance spectrometry

SEM	scanning electron microscopy
GPC	gel permeation chromatography
Mn	number-average molar masses
Mw	weight-average molar masses
DMA	dynamic mechanical analysis
Ts	tensile strength
Eb	elongation at break
E’	storage modulus
E’’	loss modulus
Tg	glass transition
AFM	atomic force microscopy
TEM	transmission electron microscopy
SAXS	small-angle X-ray scattering
TGA	thermogravimetric analysis
DVS	dynamic vapor sorption
IEC	ion exchange capacity (mmol g^{-1})
WU	water uptake (%)
SR	swelling ratio (%)
λ	hydration number
MEA	membrane electrode assembly

1. ^{1}H NMR spectra characterization.

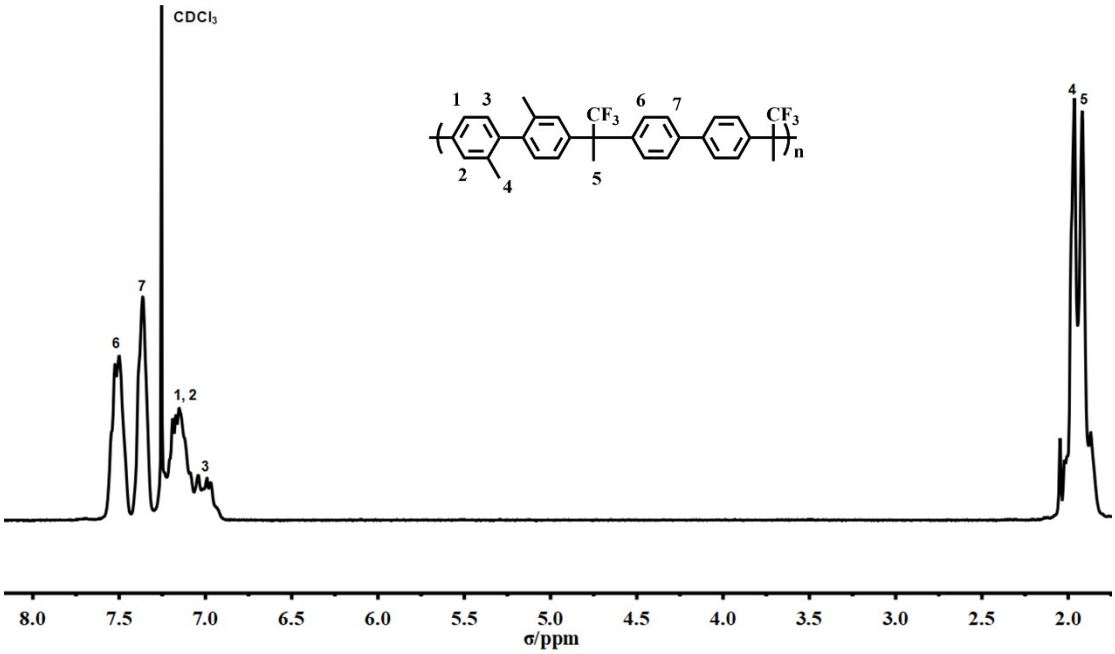

Figure S1a. ^{1}H NMR spectra (400 MHz, 298K, $CHCl_3$) of BP copolymers.

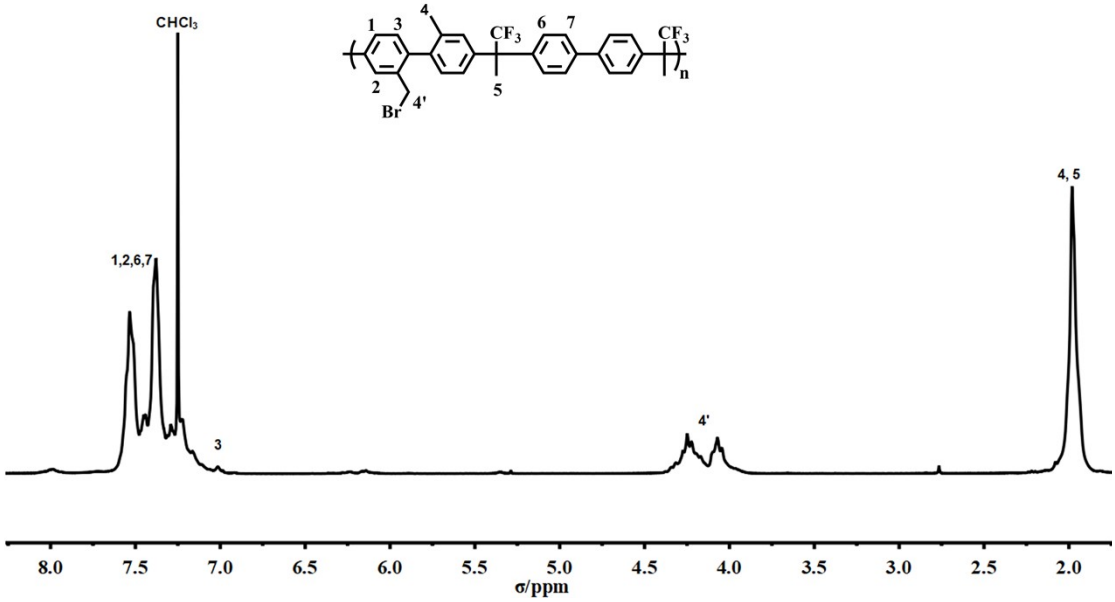

Figure S1b. ^{1}H NMR spectra (400 MHz, 298K, $CHCl_3$) of BrBP polymers.

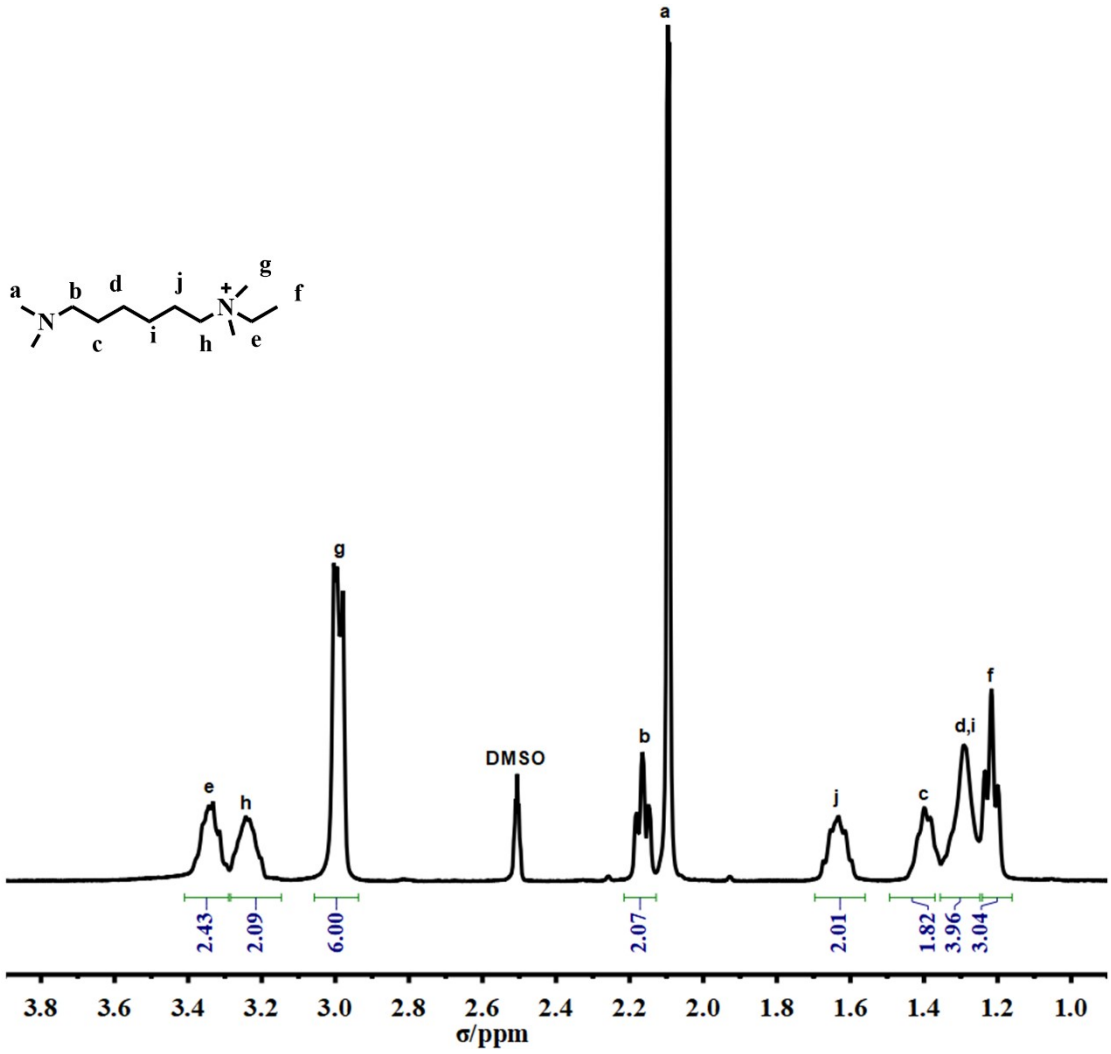

Figure S1c. [1]H NMR spectra (400 MHz, 298K, DMSO) of TMAQA.

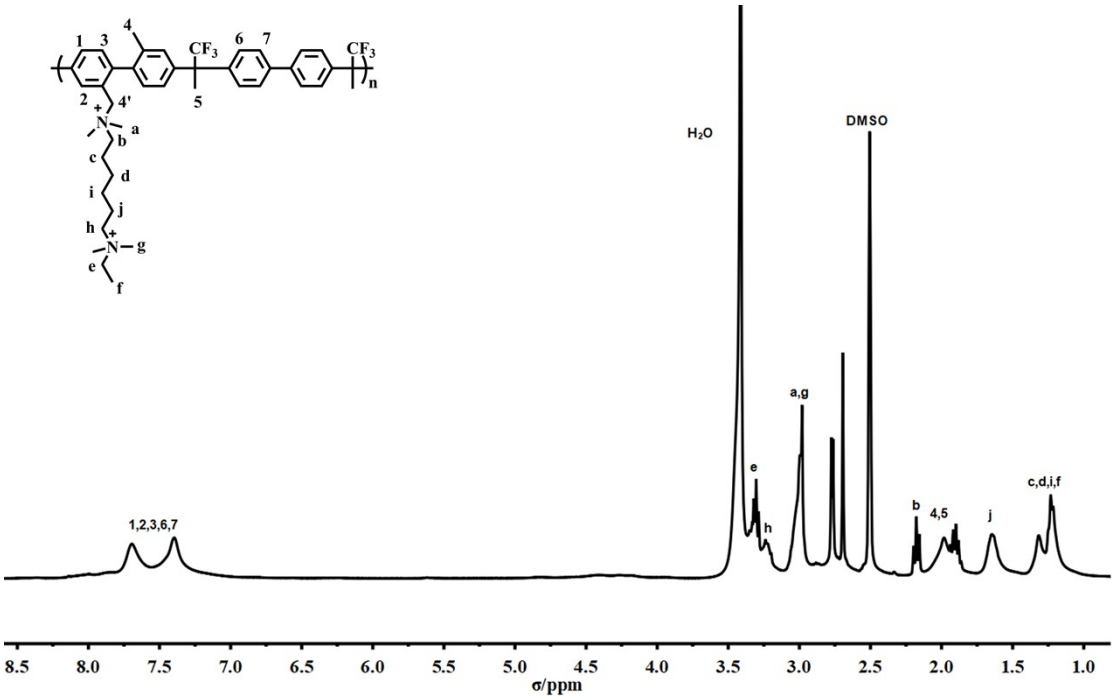

Figure S1d. [1]H NMR spectra (400 MHz, 298K, DMSO) of QABP-1 membrane.

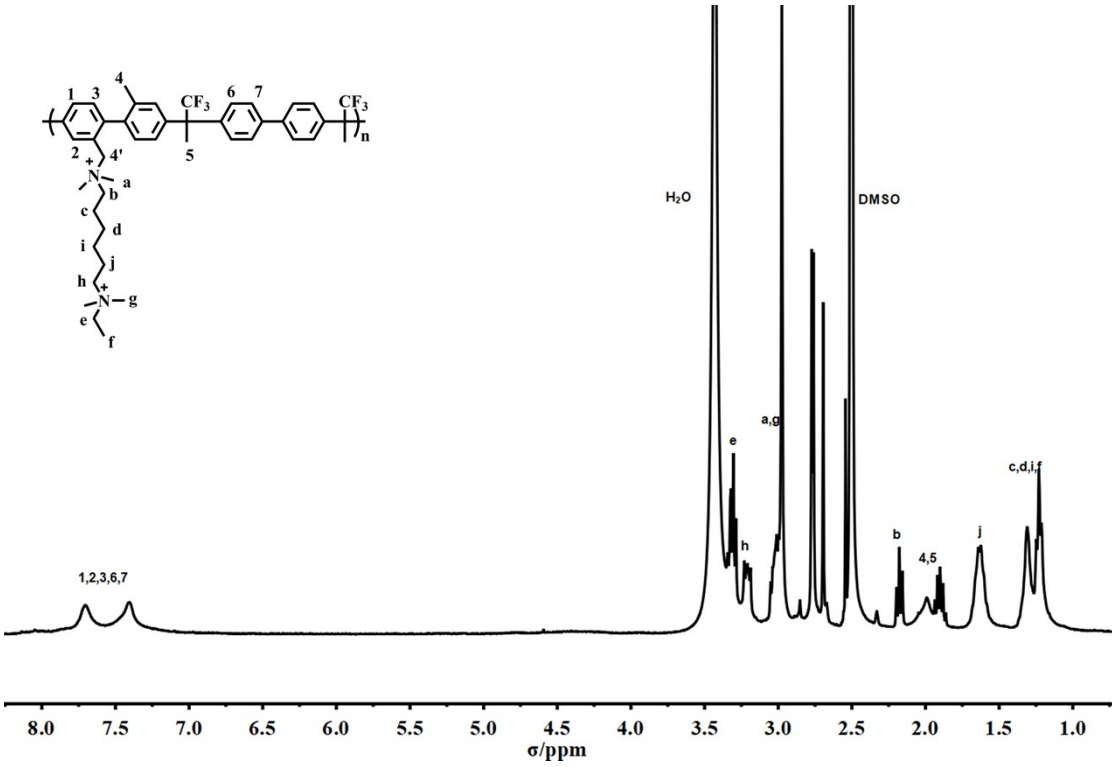

Figure S1e. [1]H NMR spectra (400 MHz, 298K, DMSO) of QABP-2 membrane.

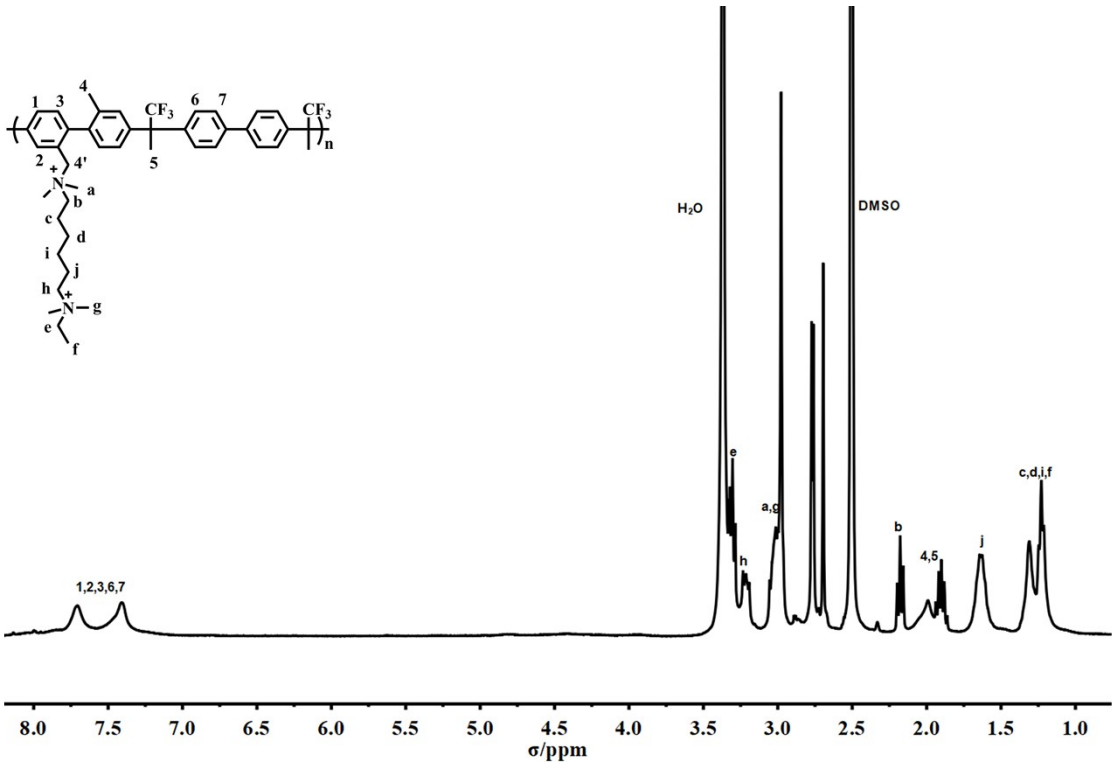

Figure S1f. [1]H NMR spectra (400 MHz, 298K, DMSO) of QABP-3 membrane.

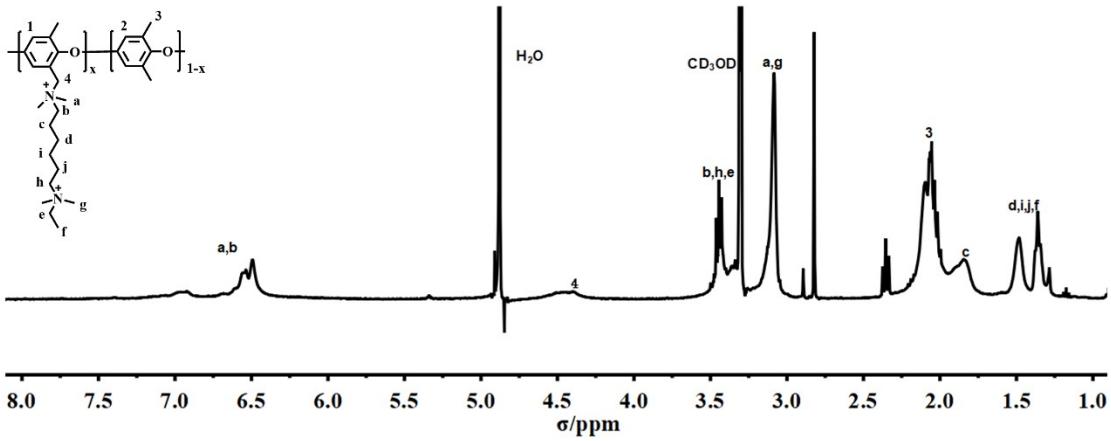

Figure S1g. ^{1}H NMR spectra (400 MHz, 298K, CD_3OH) of BQAPPO membrane

2. Experimental details.

Measurements of IEC, WU and SR. IEC was measured by the conventional method of Mohr titration. A thoroughly dried membrane sample was first weighed and then immersed in 1 mol L^{-1} NaCl aqueous solution (aq.) for 24 h. After washed with DI water for 24 h, it was immersed in 0.5 mol L^{-1} $NaSO_4$ aq. for another 24 h to release Cl^- from the membrane. Lastly, 0.1 mol L^{-1} $AgNO_3$ aq. was used to titrate the solution with K_2CrO_4 indicator. IEC was calculated as follows:

$$IEC(mmol/g) = (v_{AgNO_3} \times C_{AgNO_3})/W_{dry}$$

Membrane samples with size of 4 cm × 4 cm were dried at 80 °C for 12 h and recorded the mass and length. After that, the samples were soaked in 1 mol L^{-1} NaOH aq. for 24 h and washed with DI water. The mass and length were again recorded after wiped excess water on the membrane surface. The WU and SR were calculated according to follows:

$$Water\ Uptake(wt\%) = \frac{W_{wet} - W_{dry}}{W_{dry}} \times 100\%$$

$$Swell\ Ratio(wt\%) = \frac{L_{wet} - L_{dry}}{L_{dry}} \times 100\%$$

Measurements of hydration number (λ). The number of water molecules per QA group, denoted as λ, was calculated from the DVS data by the following equation:

$$\lambda = \frac{W}{18 \times IEC}$$

Measurements of OH^- Conductivity. Membrane samples with a size of 1 cm × 4 cm were immersed in deaerated deionized (DI) water and sealed in glass bottles for 24 h under room temperature. Then the samples were washed more than ten times with deionized water to remove lye from the membrane surface. It was quickly fixed in a Teflon cell after measured the width and thickness and immersed in a DI water bath. We used the standard four-point probe technique that operated in galvanostatic mode with an amplitude of 10 uA and frequencies from 1M Hz to 100 Hz. The impedance (R) at fully hydrated conditions and given temperature were collected on AC impedance analyzer (Zahner Zennium E). The in-plane hydroxide conductivity (σ) was calculated from the following equation:

$$\sigma = \frac{L}{Rwd}$$

where L is the distance between potential sensing electrodes, R is the measured resistance, d is the thickness of membrane and w is its width.

Estimation of the alkaline stabilities. The membrane samples were soaked in 1 mol L^{-1} NaOH aq. at 80 °C for controlled periods. Afterward, the samples were washed with DI water before measuring the OH^- conductivity.

Raman spectrum. The spectrum at each dry QABP-2 membrane sampling point was recorded with a spectral range of 1800–400 cm^{-1} using LabRamHR Evolution with the excitation wavelength λ = 785 nm (17 mW).

Solid-state NMR. The ^{13}C magic-angle spinning spectra of dried QABP-2 membrane samples were collected using the 600 MHz WB Solid-State Nuclear Magnetic Resonance Spectrometer (^1H resonance = 600 MHz, Bruker AVANCE NEO 600 WB).

Supplementary Figure.

Table S1. GPC date of BrBP and BPPO polymers.

Polymer	Retention time	Mn	Mw	Mp	Mz	Mz+1	Polydispersity index	Mz/ Mw
BrBP	18.124	89660	267648	379969	367959	433400	2.985	1.375

BPPO	19.733	22477	76076	97513	171570	273439	3.384	2.255

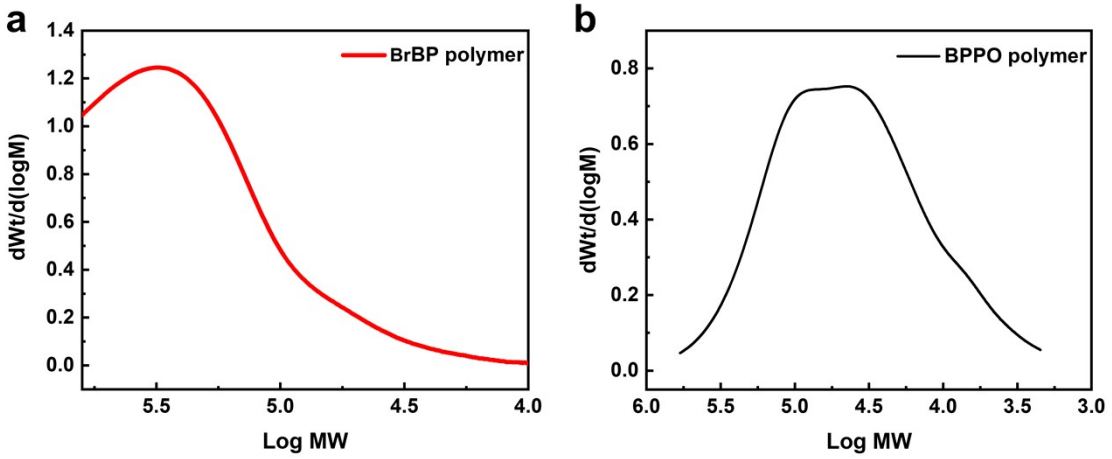

Figure S2. GPC trace of (a) BrBP polymers and (b) BPPO polymer (the mobile phase is THF).

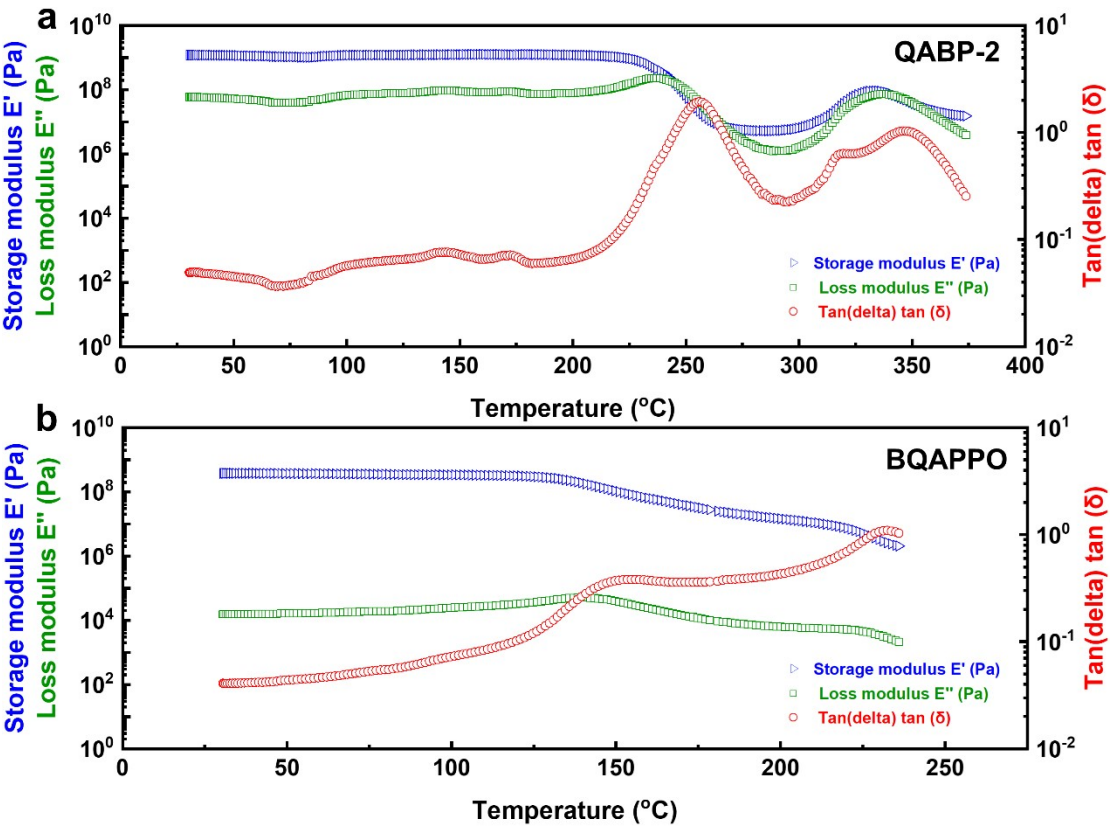

Figure S3. Dynamic mechanical analysis (DMA) profiles for (a) QABP-2 and (b) BQAPPO.

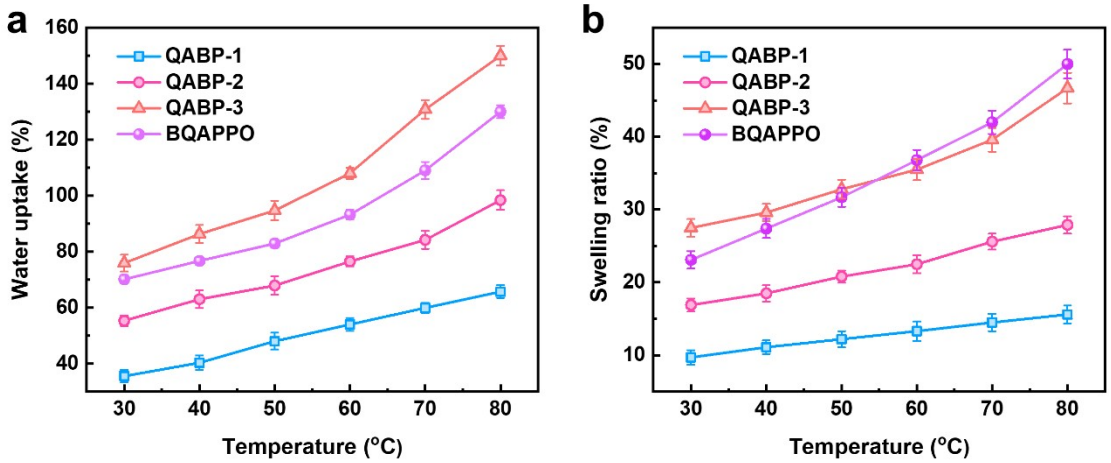

Figure S4. (a) Water uptake and (b) Swelling ratio of QABP-x and BQAPPO membranes versus temperature.

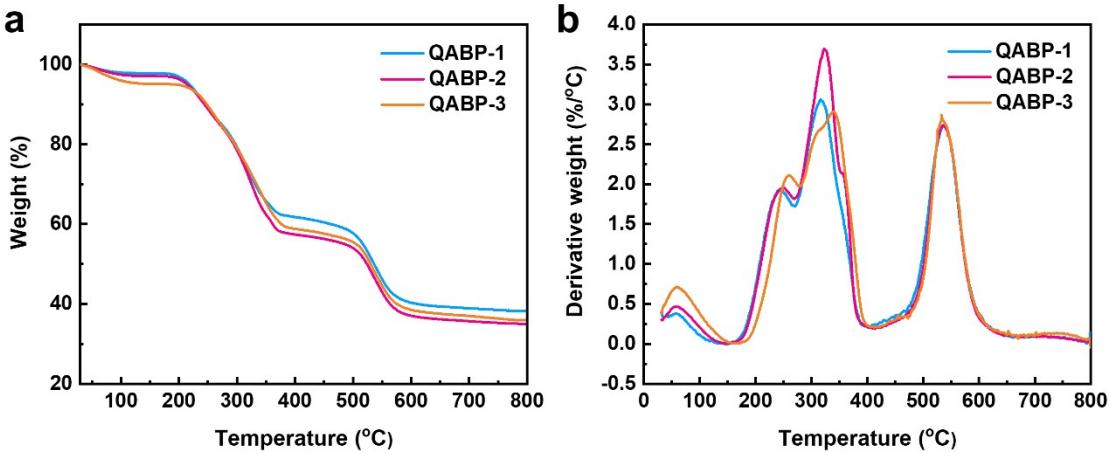

Figure S5. (a) Termogravimetric analysis (TGA) and (b) differential thermal gravity (DTG) curve of the QABP-x membranes.

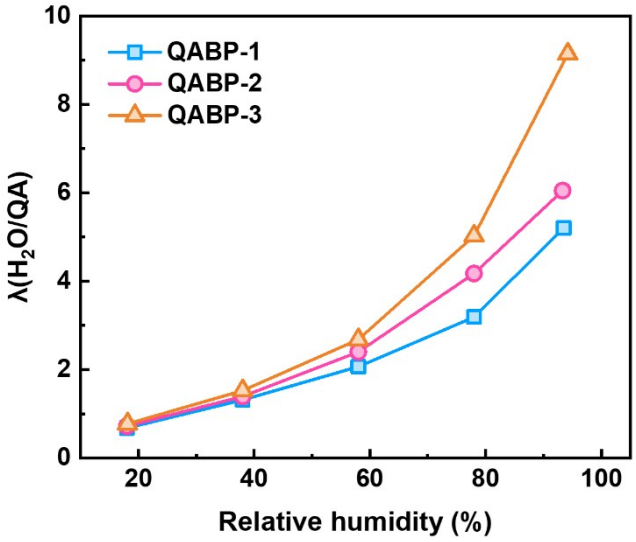

Figure S6. The hydration number of QABP-x membranes calculated from the DVS

experimental data.

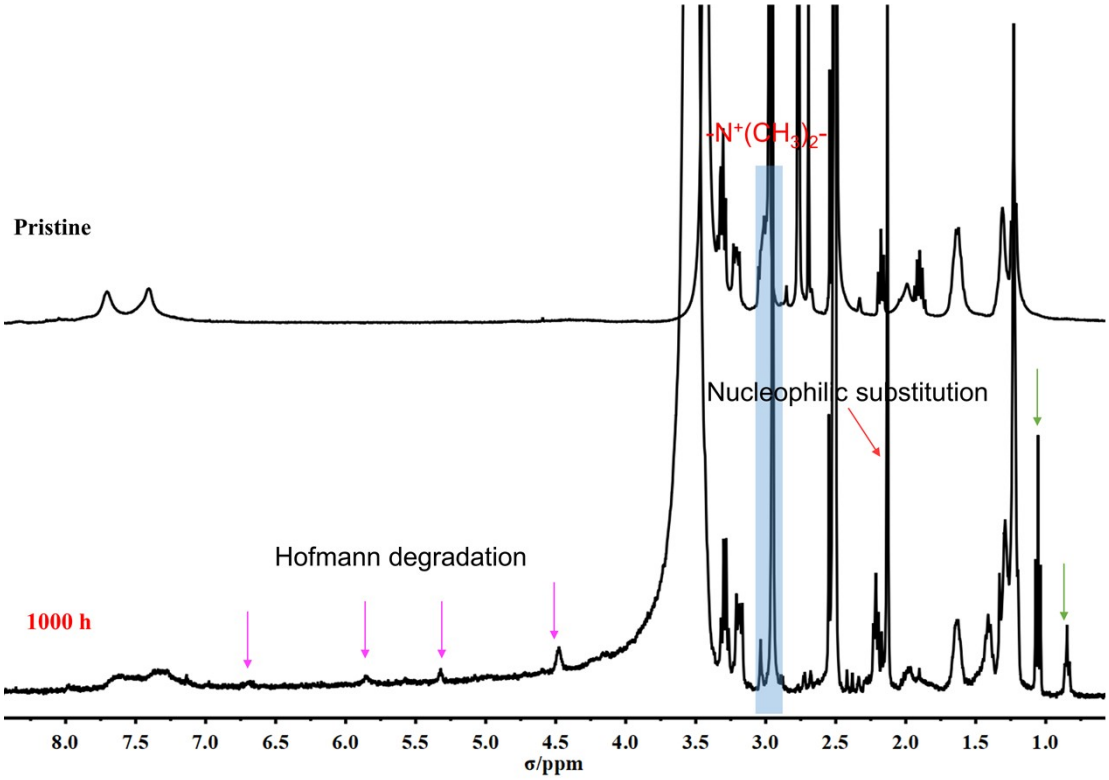

Figure S7. ^{1}H NMR spectra of a QABP-2 membrane before and after treatment in 1 M NaOH at 80 ^{o}C.

As shown in Figure S7, the peak at 3.0 ppm of QA decreases after alkaline treatment. The new signals started to appear at 5.8 ppm, 5.3 ppm is consistent with the formation of $-N^{+}(CH_3)_2–(CH_2)_4CH=CH_2$ groups on the side chains as a result of Hofmann elimination of terminal QA cations. Additionally, signals that emerge at 6.6 ppm and 4.5 ppm are also due to the Hofmann elimination[1]. Signals emerge at 2.1 ppm ascribed to the hydrogen on a tertiary amine caused by nucleophilic substitution[2]. The new signals at 1.0 ppm and 0.8 ppm ascribed to methylene on the degradation molecular[3].

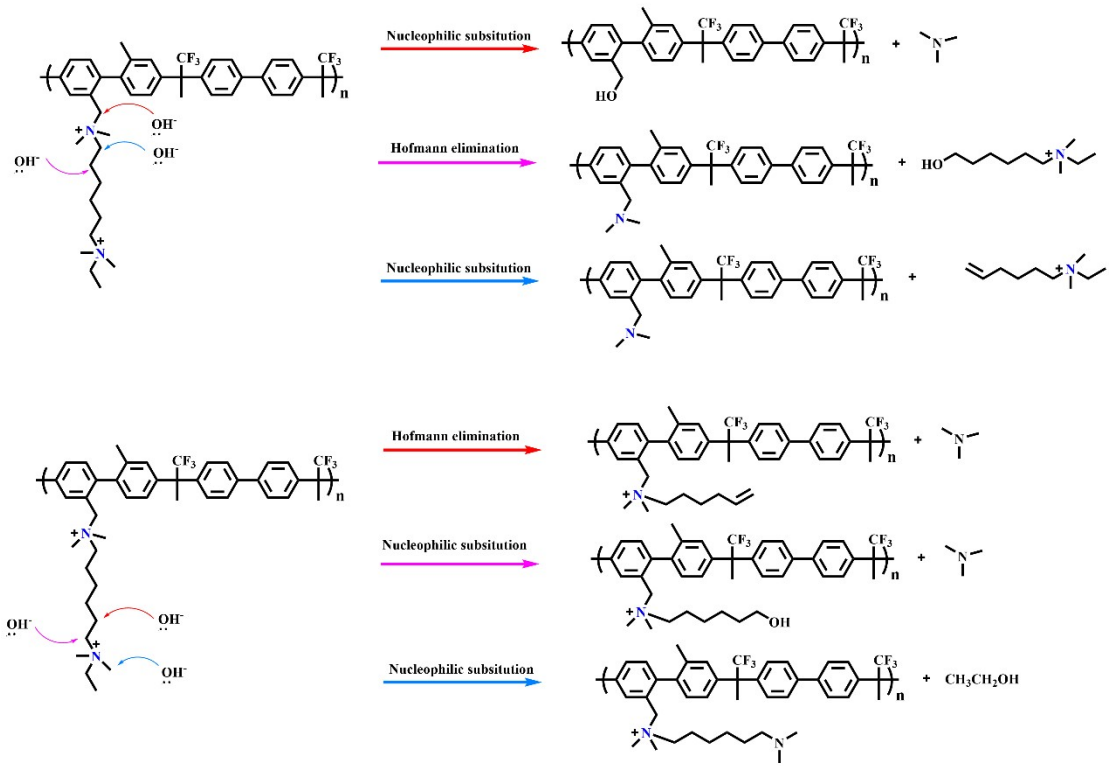

Figure S8. The possible degradation pathways of the QABP-2 AEMs under alkaline conditions (1 M NaOH aqueous solution, 80 °C).

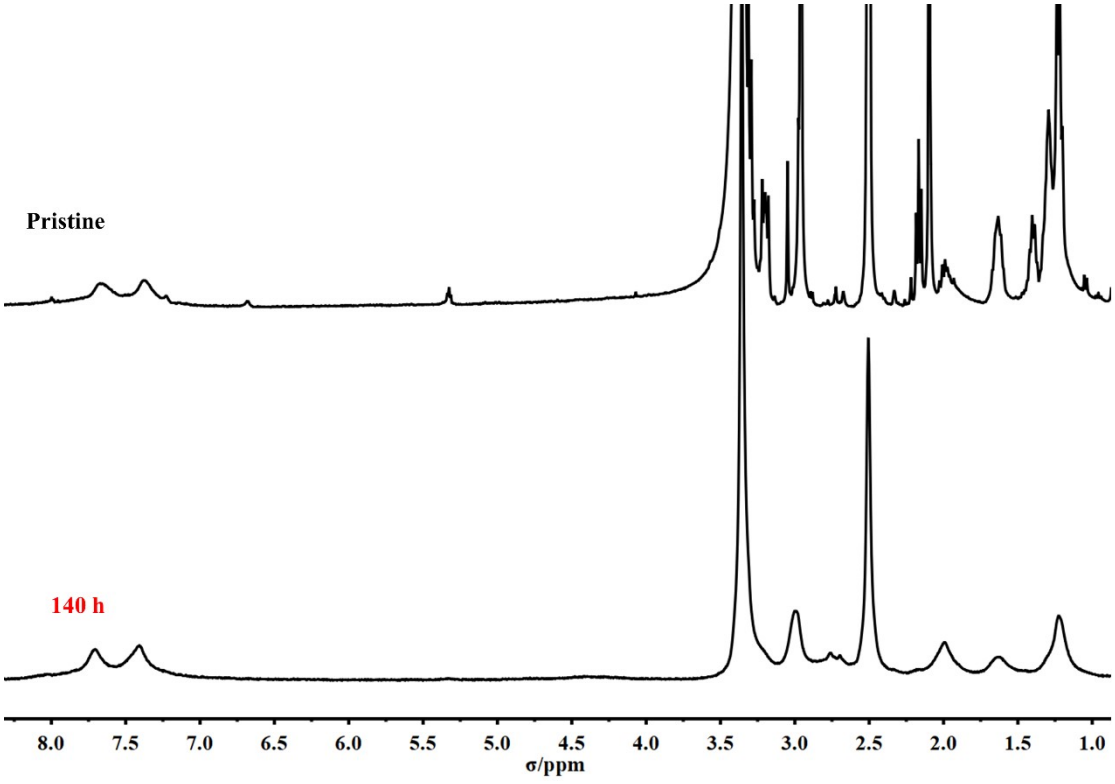

Figure S9. ^{1}H NMR spectra of a QABP-2 membrane before and after long-term

durability test of fuel cells for 140 h.

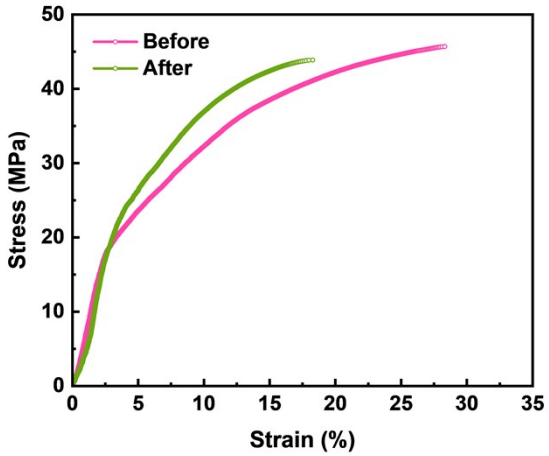

Figure S10. The mechanical properties (in OH^- form and wet state) of QABP-2 in 1 M NaOH at 80 °C for 1000 h.

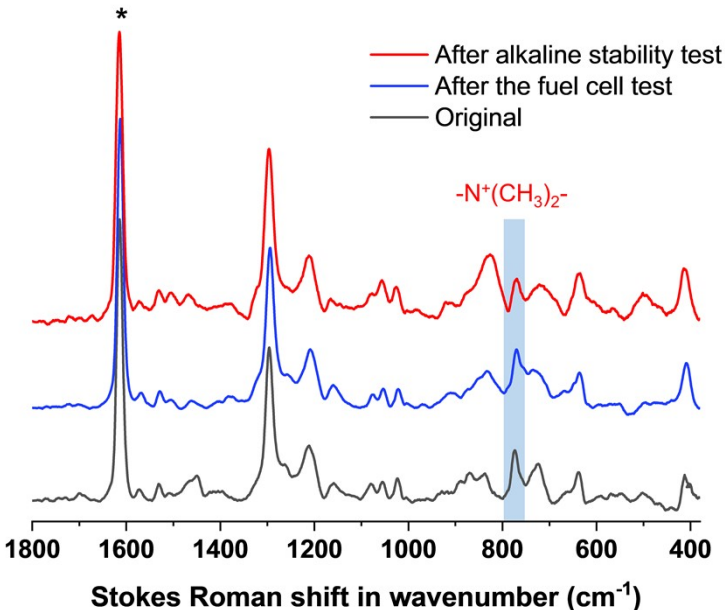

Figure S11. The Raman spectra of (a) QABP-2 before (bottom spectrum) and after operating in fuel cell (middle spectrum) and after alkaline stability test in 1 M NaOH at 80 °C (top spectrum); All spectral intensities are normalized to the peak labeled * to aid in visual comparison.

As shown in **Figure S11**, almost no changes to the aromatic peaks (1615, 1295, and 1212 cm^{-1}) are observed for the AEM after alkaline stability and fuel cell operation. Additionally, the photos taken after the alkaline stability test (**Fig 4d**) and the stress-strain test **(Figure S10)** also show that the visual appearance and mechanical strength

of the AEM have hardly changed. These suggest the integrity of the aggregate backbone. But, the ammonium (QA) peak at 774 cm^{-1} shows a decreased intensity for the AEM after alkaline stability while minor changes to the AEM after the fuel cell test. This suggests that the OH^- nucleophilic attack results in the loss of the QA group. The operation time of 140 hours doesn't result in the obvious degradation of QA groups.

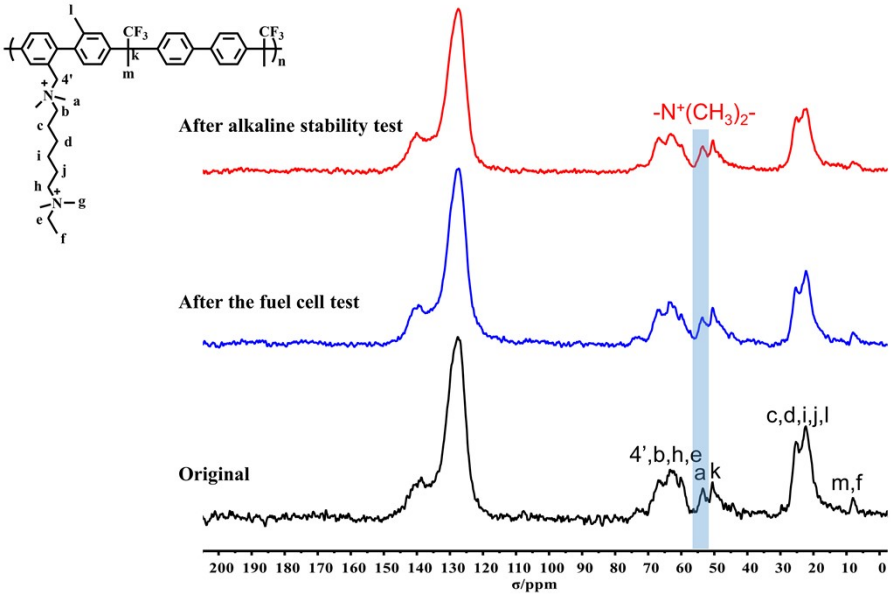

Figure S12. The ^{13}C solid-state NMR of QABP-2 before (bottom spectrum) and after operating in fuel cell (middle spectrum) and after alkaline stability test in 1 M NaOH at 80 ^oC (top spectrum); Magic angle spinning rotation rate = 22 kHz. All spectra were normalized to the intensity of the d = 127 ppm peak to aid visual comparison.

The ^{13}C solid-state NMR spectra of the degraded QABP-2 are shown in Figure S12. The resonance line at σ = 138.6 ppm and 127 ppm correspond to the polymer-bound rings and -CF_3-, and no intensity change occurs after the fuel cell and alkaline stability test. A slight decrease in intensity of the band corresponding to the quaternary ammonium methylene carbons (σ = 53). Additionally, the signal of benzylic (σ = 69) and methylene (σ = 8, 22.3-25.2, 60.1-66.8) in the side chains are weakened. This indicates that not only part of the QA group but also part of the benzyl group grafting was lost during the alkali treatment. Altogether, the solid-state NMR observations indicate a low level of AEM degradation, consistent with the Raman data discussed above.

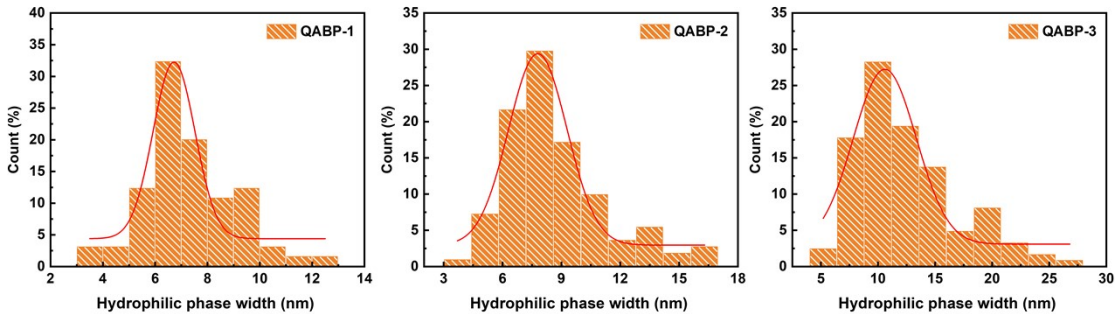

Figure S13. The distribution of hydrophilic phase width of QABP-x analyzed by the Nano Measurer.

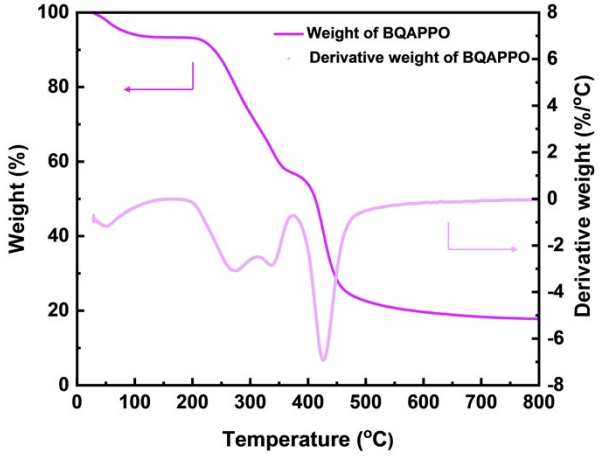

Figure S14. Termogravimetric analysis (TGA) and differential thermal gravity (DTG) curve of the QABPPO membrane.

Table S2. Summary and comparison of representative AEMFCs performance.

Year	AEM	A/C Ionomer	Anode	Cathode	A/C Metal loading (wt%)	A/C Fuel	Cell temperature (°C)	A/C Back pressure（MPa）	Power density (W cm^{-2})	Durability (h)	Reference
Ultrathin AEMs											
2013	xQAPS@PTFE-25um	TQAPS	Pt/C	Pt/C	0.4/0.4	H_2/O_2	60	0.1	0.55	NA	[4]
2018	QAPEEK/s-NBF-15um	QAPEEK	PtRu/C	Pt/C	0.4/0.4	H_2/O_2	60	0.1	0.93	NA	[5]
2018	LDPE15-15um	ETFE-based RG	PtRu/C	Pt/C	0.4/0.4	H_2/O_2	80	0	2.02	20	[6]
2020	GTR75-15 -10um	GT32 and GT73	PtRu/C	Pt/C	0.672/0.584	H_2/O_2	80	0	3.21	0	[7]
2020	DMD-5um	HMT-PMBI	PtRu/C	Pt/C	0.3/0.3	H_2/O_2	70	0	1.0	20	[8]
2021	cQAPPT -10um	QAPPT	Pt/C	Pt/C	0.4/0.4	H_2/O_2	80	0.2	1.85	NA	[9]
2021	2-ACPBI -10um	homemade ionomer	Pt/C	Pt/C	0.5/0.5	H_2/O_2	80	0.1	0.63	10	[10]
2021	Tec-PBI-50 -10um	Tec-PBI-50	Pt/C	Pt/C	0.5/0.5	H_2/O_2	80	0.15	1.16	10	[11]
2021	xTQA50-17um	S29QA30	Pt/C	Pt/C	NA	H_2/O_2	60	0	0.405	NA	[12]
2022	UHMWPE10-s-10um	PAP-BP-60	PtRu/C	Pt/C	0.5/0.5	H_2/O_2	65	0.15	0.709	10	[13]

2022	PQP-100-10um PQP-100-4um	PBP-67	Pt/C	Pt/C	0.5/0.5	H_2/O_2	60	0	0.45 0.417	NA	[14]
2022	QABP-2	QABP-3	PtRu/C	Pt/C	0.5/0.5	H_2/O_2	80	0.2	1.8	140	This work
Side chain type AEMs											
2019	CPFBP-TQA-100	NA	Pt/C	Pt/C	NA	H_2/O_2	80	0	0.116	24	[15]
2019	F20C9N	ETFE-g-poly(VBTMAC)	PtRu/C	Pt/C	NA	H_2/O_2	60	0	1.01	120	[16]
2020	PES–NS-10%	NA	Pt/C	Pt/C	NA	H_2/O_2	60	0	0.11	24	[17]
2020	TQ-PDBA-70%	NA	Pt/C	Pt/C	NA	H_2/O_2	80	0	0.16	48	[18]
2020	QPC-TMA	QPC-TMA	PtRu/C	Pt/C	0.4/0.4	H_2/O_2	60	0	1.61	NA	[19]
2022	P(4PA-co-2PA)-47	FLN-55	Pt/C	Pt/C	0.5/0.5	H_2/O_2	80	0.1	0.4	100	[20]

Table S3. Summary and comparison of the most important properties of AEMs.

Year	AEM	IEC (mmol g^{-1})	Tensile strength (MPa)	Elongation at break (%)	Water uptake [a] (%)	Swelling ratio [a] (%)	OH^- Conductivity [b] (mS cm^{-1})	Alkaline stability time [c] (h)	Reference
2013	xQAPS@PTFE	1.23	31.1	NA	NA	0	28 (60 °C)	NA	[4]
2017	XE-Imd70	2.72	60.2	23.7	58 (20 °C)	62 (80 °C)	28-103	510	[21]
2018	QAPEEK/s-NBF	1.76	15.2	NA	67	7.5	21.4-119	120	[5]
2018	LDPE15	2.54	23	71	149	27	100-210	500	[6]
2019	CPFBP-TQA-100	1.94	11.0	9.6	28.9	22.0	28.89-76.85	500 (2 M)	[15]
2019	F20C9N	1.12	NA	NA	109 (25 °C)	26 (25 °C)	23-91	1000	[16]
2020	GTR75-15	3.47	NA	NA	73 (25 °C)	16 (25 °C)	68-152	1050	[7]
2020	PES–NS-10%	1.7	35.13	3.37	13.33	5.77	40-90	864 (2 M)	[17]
2020	TQ-PDBA-70%	2.16	33.42	14.43	10.84	3.23	36-137	1000	[18]
2020	QPC-TMA	2.31	NA	NA	28 (25 °C)	9 (25 °C)	77-154	1000	[19]
2021	cQAPPT	1.8	27	22	15	12.5	34-70	168	[9]

2021	2-ACPBI	1.75	14	79	32.3	8.6	50-91.2	480 (2 M)	[10]
2021	Tec-PBI-50	3.10	14	65	67.5	20	63.2-131.8	672 (2 M, 60 °C)	[11]
2021	xTQA50-PPO-SEBS	1.43	34	65	67.2 (20 °C)	9.1 (20 °C)	43.1-89.9	500	[12]
2022	UHMWPE4-s-AERM10%	1.51	155.4	53.6	9.3	NA	31-102	1440	[13]
2022	PQP-100	2.3	83.9	15.8	20.0	20.6	56.7-118.7	1344	[14]
2022	P(4PA-co-2PA)-47	2.07	39.1	11.2	13.6	1.5	30-75	720	[20]
2022	QABP-2	2.01	45.7	28.3	55.3	16.9	69-123	1000	This work

[a] Measured in 30 °C;
[b] Measured from 30 °C to 80 °C;
[c] Measured in 1 M NaOH/KOH at 80 °C.

Table S4 Summary of the gas permeability of AEMs.

AEM	H_2 permeability	O_2 permeability	Reference
xTQA50-PPO-SEBS	13.5 barrer	NA	[12]
UHMWPE4-s-AERM10%	0.06 ($10*10^{-13}$ mol/(KPa*s*cm))	NA	[13]
PQP-100	0.57 barrer/cm	0.023 barrer/cm	[14]
PAP-TP-85	$2.4*10^{-13}$ mol/(KPa*s*cm))	$0.6*10^{-13}$ mol/(KPa*s*cm))	[22]
BQAPPO	1.94 (cm^3 cm^2 min^{-1})	1.005 (cm^3 cm^2 min^{-1})	This work
QABP-2	1.57 (cm^3 cm^2 min^{-1})	m^3 cm^2 min^{-1})	This work

References

1. H.-S. Dang and P. Jannasch, *Journal of Materials Chemistry A*, 2016, **4**, 17138-17153.
2. A. M. Ahmed Mahmoud and K. Miyatake, *Journal of Materials Chemistry A*, 2018, **6**, 14400-14409.
3. S. A. Nuñez, C. Capparelli and M. A. Hickner, *Chemistry of Materials*, 2016, **28**, 2589-2598.
4. G. Li, J. Pan, J. Han, C. Chen, J. Lu and L. Zhuang, *Journal of Materials Chemistry A*, 2013, **1**.
5. Y. Peng, Y. Wang, X. Wei, J. Zhou, H. Peng, L. Xiao, J. Lu and L. Zhuang, *ACS Appl Mater Interfaces*, 2018, **10**, 33581-33588.
6. L. Wang, M. Bellini, H. A. Miller and J. R. Varcoe, *Journal of Materials Chemistry A*, 2018, **6**, 15404-15412.
7. M. Mandal, G. Huang, N. U. Hassan, W. E. Mustain and P. A. Kohl, *Journal of Materials Chemistry A*, 2020, **8**, 17568-17578.
8. P. Veh, B. Britton, S. Holdcroft, R. Zengerle, S. Vierrath and M. Breitwieser, *RSC Adv*, 2020, **10**, 8645-8652.
9. S. Chen, H. Peng, M. Hu, G. Wang, L. Xiao, J. Lu and L. Zhuang, *ACS Applied Energy Materials*, 2021, **4**, 4297-4301.
10. X. Wang, J. Li, W. Chen, B. Pang, Y. Liu, Y. Guo, X. Wu, F. Cui and G. He, *ACS Appl Mater Interfaces*, 2021, **13**, 49840-49849.
11. X. Wang, W. Chen, T. Li, X. Yan, Y. Zhang, F. Zhang, X. Wu, B. Pang, J. Li and G. He, *Journal of Materials Chemistry A*, 2021, **9**, 7522-7530.
12. S. Sung, J. E. Chae, K. Min, H.-J. Kim, S. Y. Nam and T.-H. Kim, *Journal of Materials Chemistry A*, 2021, **9**, 1062-1079.
13. W. Yuan, L. Zeng, Y. Li, J. Wang, X. Wang, Q. Liao, L. Li and Z. Wei, *Small*, 2022, **18**, e2105499.
14. M. Liu, X. Hu, B. Hu, L. Liu and N. Li, *Journal of Membrane Science*, 2022, **642**.
15. H. Y. Wu, Q. Yang, X. L. Gao, Z. Y. Zhu, Q. H. Sun, Q. G. Zhang, A. M. Zhu and Q. L. Liu, *Electrochimica Acta*, 2019, **321**.

16. L. Zhu, X. Peng, S. L. Shang, M. T. Kwasny, T. J. Zimudzi, X. Yu, N. Saikia, J. Pan, Z. K. Liu, G. N. Tew, W. E. Mustain, M. Yandrasits and M. A. Hickner, *Advanced Functional Materials*, 2019, **29**.
17. F. H. Liu, Q. Yang, X. L. Gao, H. Y. Wu, Q. G. Zhang, A. M. Zhu and Q. L. Liu, *Journal of Membrane Science*, 2020, **595**.
18. X. L. Gao, L. X. Sun, H. Y. Wu, Z. Y. Zhu, N. Xiao, J. H. Chen, Q. Yang, Q. G. Zhang, A. M. Zhu and Q. L. Liu, *Journal of Materials Chemistry A*, 2020, **8**, 13065-13076.
19. M. S. Cha, J. E. Park, S. Kim, S.-H. Han, S.-H. Shin, S. H. Yang, T.-H. Kim, D. M. Yu, S. So, Y. T. Hong, S. J. Yoon, S.-G. Oh, S. Y. Kang, O.-H. Kim, H. S. Park, B. Bae, Y.-E. Sung, Y.-H. Cho and J. Y. Lee, *Energy & Environmental Science*, 2020, **13**, 3633-3645.
20. T. Jiang, C. Wu, Y. Zhou, S. Cheng, S. Yang, H. Wei, Y. Ding and Y. Wu, *Journal of Membrane Science*, 2022, **647**.
21. K. H. Lee, D. H. Cho, Y. M. Kim, S. J. Moon, J. G. Seong, D. W. Shin, J.-Y. Sohn, J. F. Kim and Y. M. Lee, *Energy & Environmental Science*, 2017, **10**, 275-285.
22. J. Wang, Y. Zhao, B. P. Setzler, S. Rojas-Carbonell, C. Ben Yehuda, A. Amel, M. Page, L. Wang, K. Hu, L. Shi, S. Gottesfeld, B. Xu and Y. Yan, *Nature Energy*, 2019, **4**, 392-398.